PNAS INAUGURAL ARTICLE | APPLIED PHYSICAL SCIENCES

Mechanical theory of nonequilibrium coexistence and motility-induced phase separation

Ahmad K. Omar[a,b,1,2], Hyeongjoo Row[c,1], Stewart A. Mallory[d,1], and John F. Brady[c,2]

This contribution is part of the special series of Inaugural Articles by members of the National Academy of Sciences elected in 2020.
Contributed by John F. Brady; received November 21, 2022; accepted March 24, 2023; reviewed by Hartmut Loewen, M. Cristina Marchetti, and Ignacio Pagonabarraga

Nonequilibrium phase transitions are routinely observed in both natural and synthetic systems. The ubiquity of these transitions highlights the conspicuous absence of a general theory of phase coexistence that is broadly applicable to both nonequilibrium and equilibrium systems. Here, we present a general mechanical theory for phase separation rooted in ideas explored nearly a half-century ago in the study of inhomogeneous fluids. The core idea is that the mechanical forces within the interface separating two coexisting phases uniquely determine coexistence criteria, regardless of whether a system is in equilibrium or not. We demonstrate the power and utility of this theory by applying it to active Brownian particles, predicting a quantitative phase diagram for motility-induced phase separation in both two and three dimensions. This formulation additionally allows for the prediction of novel interfacial phenomena, such as an increasing interface width while moving deeper into the two-phase region, a uniquely nonequilibrium effect confirmed by computer simulations. The self-consistent determination of bulk phase behavior and interfacial phenomena offered by this mechanical perspective provide a concrete path forward toward a general theory for nonequilibrium phase transitions.

nonequilibrium | phase diagram | active matter | driven assembly | coexistence

Significance

Phase separation, the coexistence between distinct macroscopic phases (such as oil coexisting with water), is ubiquitous in everyday life and motivated the development of the equilibrium theory of coexistence by Maxwell, van der Waals, and Gibbs. However, phase separation is increasingly observed in both synthetic and living nonequilibrium systems, where thermodynamic principles are strictly inapplicable. Here, we develop a mechanical description of phase separation, offering a route for constructing phase diagrams without presuming equilibrium Boltzmann statistics. We highlight the utility of our approach by developing a first-principles theory for motility-induced phase separation and the uniquely nonequilibrium interfacial phenomena that accompany this transition.

The diversity of phase behavior and pattern formation found in far-from-equilibrium systems has brought renewed focus to the theory of nonequilibrium phase transitions. Intracellular phase separation resulting in membraneless organelles (1, 2) and pattern formation on cell surfaces (3) are just a few instances in which nonequilibrium phase transitions are implicated in biological function. Colloids (4) and polymers (5–8) subject to boundary-driven flow can experience shear-induced phase transitions and patterns that profoundly alter their transport properties. Microscopic self-driven particles, such as catalytic Janus particles, motile bacteria, or field-directed synthetic colloids, exhibit phase transitions eerily similar to equilibrium fluids despite the absence of traditional equilibrium driving forces (9–14).

A general predictive framework for constructing phase diagrams for these driven systems is notably absent. For equilibrium systems, the formulation of a theory for phase coexistence was among the earliest accomplishments in thermodynamics. Maxwell (15), building on the work of van der Waals, derived what are now familiar criteria for phase equilibria for a one-component system: equality of temperature, chemical potential, and pressure. These criteria are rooted in the fundamental equilibrium requirements that free energy be extensive and convex for any unconstrained degrees of freedom within a system. The lack of such a variational principle for nonequilibrium systems has limited the theoretical description of out-of-equilibrium phase transitions.

The absence of a general theory for nonequilibrium coexistence has been particularly evident in the field of active matter. The phenomenon of motility-induced phase separation (MIPS)—the occurrence of liquid–gas phase separation among repulsive active Brownian particles (ABPs)—has motivated a variety of perspectives (16–26) in pursuit of a theory for active coexistence. These perspectives range from kinetic models (27), continuum and generalized Cahn–Hilliard approaches (16, 18, 28), large deviation theory (29, 30), and power functional theory (24, 25). Some of these approaches appeal to equilibrium notions such as free energy and chemical potential (19), concepts which lack a rigorous basis for active systems. Without a first-principles nonequilibrium coexistence theory, one cannot compare or assess the various perspectives. Despite the significant progress, a closed-form theory for the coexistence criteria for MIPS, which makes no appeals to equilibrium ideas, remains an outstanding challenge in the field.

Author contributions: A.K.O., H.R., S.A.M., and J.F.B. designed research; performed research; contributed new reagents/analytic tools; analyzed data; and wrote the paper.

Reviewers: H.L., Heinrich-Heine-Universität Düsseldorf; M.C.M., University of California, Santa Barbara; and I.P., University of Barcelona.

The authors declare no competing interest.

[1]A.K.O., H.R., and S.A.M. contributed equally to this work.

[2]To whom correspondence may be addressed. Email: aomar@berkeley.edu or jfbrady@caltech.edu.

This article contains supporting information online at http://www.pnas.org/lookup/suppl/doi:10.1073/pnas.2219900120/-/DCSupplemental.

Published April 24, 2023.

Mechanics is a natural choice for describing the behavior of both equilibrium and nonequilibrium systems as it is agnostic to the underlying distribution of microstates. In this article, we construct an entirely mechanical description of liquid–gas coexistence, relying only on notions such as forces and stresses. This formulation is an extension of the mechanical perspective developed decades ago to describe coexistence and interfacial phenomena for equilibrium systems (31–33). We highlight the utility of this framework by developing a theory for the coexistence criteria of MIPS and comparing our theory's predictions to results from computer simulation. Our formulation further allows for the prediction of novel nonequilibrium interfacial behavior, such as a nonmonotonic interfacial width, as the system is taken deeper into the coexistence region.

The Mechanics of Nonequilibrium Coexistence

We briefly review the thermodynamics of phase separation for a one-component system undergoing a liquid–gas phase transition. The order parameter distinguishing the liquid and gas phases is the number density $\rho \equiv N/V$, where N and V are the number of particles and volume, respectively. For simple substances at a uniform temperature T below a critical temperature T_c, the mean-field Helmholtz free energy $\mathcal{F}(N, V, T)$ becomes concave for a range of densities, in violation of thermodynamic stability. The system resolves this instability by separating into coexisting macroscopic domains of liquid and gas with densities ρ^{liq} and ρ^{gas}, respectively. The free energy of the phase-separated system (neglecting interfacial free energy) is now $V^{\text{liq}}f(\rho^{\text{liq}}, T) + V^{\text{gas}}f(\rho^{\text{gas}}, T)$ where we have defined the free energy density $f(\rho, T) \equiv \mathcal{F}(N, V, T)/V$. The volumes occupied by the liquid (V^{liq}) and gas (V^{gas}) phases sum to the total system volume V. We now obtain the coexistence criteria by minimizing the total free energy with respect to ρ^{liq} and ρ^{gas} subject to the conservation of particle number constraint (i.e., $V^{\text{liq}}\rho^{\text{liq}} + V^{\text{gas}}\rho^{\text{gas}} = V\rho$). This results in the familiar coexistence criteria:

$$\begin{aligned} \mu(\rho^{\text{liq}}, T) = \mu(\rho^{\text{gas}}, T) = \mu^{\text{coexist}}(T), \\ p(\rho^{\text{liq}}, T) = p(\rho^{\text{gas}}, T) = p^{\text{coexist}}(T), \end{aligned} \quad \textbf{[1a]}$$

where $\mu(\rho, T) = \partial f(\rho, T)/\partial\rho$ is the chemical potential, $p(\rho, T) = -f(\rho, T) + \rho\mu(\rho, T)$ is the pressure, and $\mu^{\text{coexist}}(T)$ and $p^{\text{coexist}}(T)$ are the coexistence values for the chemical potential and pressure, respectively, at the temperature of interest. It is straightforward to show that Eq. **1a** can be equivalently expressed as

$$\begin{aligned} \mu(\rho^{\text{liq}}) = \mu(\rho^{\text{gas}}) = \mu^{\text{coexist}}, \\ \int_{\rho^{\text{gas}}}^{\rho^{\text{liq}}} \left[\mu(\rho) - \mu^{\text{coexist}}\right] d\rho = 0, \end{aligned} \quad \textbf{[1b]}$$

or similarly

$$\begin{aligned} p(\upsilon^{\text{liq}}) = p(\upsilon^{\text{gas}}) = p^{\text{coexist}}, \\ \int_{\upsilon^{\text{gas}}}^{\upsilon^{\text{liq}}} \left[p(\upsilon) - p^{\text{coexist}}\right] d\upsilon = 0, \end{aligned} \quad \textbf{[1c]}$$

where we have defined the inverse density $\upsilon \equiv 1/\rho$ and have dropped the dependence on T in Eqs. **1b** and **1c** for convenience.

The integral expressions in Eqs. **1b** and **1c** are often referred to as equal-area or Maxwell constructions (15) in the $\mu-\rho$ and $p-\upsilon$ planes, respectively. These expressions are equivalent to Eq. **1a** and can be used to compute the coexistence curve or binodal as a function of T. The spinodal boundaries enclose the region of the phase diagram in which thermodynamic stability is violated, i.e., $(\partial^2 f/\partial\rho^2)_T < 0$ or equivalently when $(\partial p/\partial\rho)_T < 0$ or $(\partial\mu/\partial\rho)_T < 0$. These boundaries can thus be determined by finding the densities at which $(\partial p/\partial\rho)_T = 0$ or $(\partial\mu/\partial\rho)_T = 0$ for a specified temperature.

Interestingly, the coexistence criteria presented in Eq. **1c** contains only the mechanical equation-of-state, a quantity which is readily defined for nonequilibrium systems (unlike, for example, chemical potential). In fact, Eq. **1c** has been used in previous studies (19, 34) to obtain the phase diagram of active systems. However, its validity for nonequilibrium systems is questionable as its origins are clearly rooted in a variational principle that holds only for equilibrium systems.

We are now poised to construct a theory of coexistence based purely on mechanics. As previously noted, the order parameter for liquid–gas phase separation is density. The evolution equation for the order parameter is therefore simply the continuity equation:

$$\frac{\partial\rho}{\partial t} + \boldsymbol{\nabla}\cdot\mathbf{j}^{\rho} = 0, \quad \textbf{[2]}$$

where we are now considering a density field $\rho(\mathbf{x}; t)$ that is continuous in spatial position $\mathbf{x}$ (with $\boldsymbol{\nabla} = \partial/\partial\mathbf{x}$) and $\mathbf{j}^{\rho}(\mathbf{x}; t)$ is the number density flux. A constitutive equation for the number density flux follows directly from linear momentum conservation. This connection can be appreciated by noting that $\mathbf{j}^{\rho}(\mathbf{x}; t) \equiv \rho(\mathbf{x}; t)\mathbf{u}(\mathbf{x}; t)$ (where $\mathbf{u}(\mathbf{x}; t)$ is the number average velocity of particles) and is therefore proportional to the momentum density by a factor of the particle mass m. Expressing linear momentum conservation with $\mathbf{j}^{\rho}$ (rather than the more traditional $\mathbf{u}$),

$$\frac{\partial(m\mathbf{j}_{\rho})}{\partial t} + \boldsymbol{\nabla}\cdot(m\mathbf{j}^{\rho}\mathbf{j}^{\rho}/\rho) = \boldsymbol{\nabla}\cdot\boldsymbol{\sigma} + \mathbf{b}, \quad \textbf{[3]}$$

where $\boldsymbol{\sigma}(\mathbf{x}; t)$ is the stress tensor and $\mathbf{b}(\mathbf{x}; t)$ are the body forces acting on the particles. In simple systems, Eqs. **2** and **3** may constitute a closed set of coupled equations describing the temporal and spatial evolution of the density profile. However, the precise form of the stresses and body forces may depend on other fields, which will require additional conservation equations to furnish a closed set of equations.

As we are interested in scenarios in which phase separation reaches a stationary state of coexistence, the continuity equation reduces to $\boldsymbol{\nabla}\cdot\mathbf{j}^{\rho} = 0$, and linear momentum conservation is now $\boldsymbol{\nabla}\cdot(m\mathbf{j}^{\rho}\mathbf{j}^{\rho}/\rho) = \boldsymbol{\nabla}\cdot\boldsymbol{\sigma} + \mathbf{b}$. While $\mathbf{j}^{\rho} = \mathbf{0}$ for systems in equilibrium, nonequilibrium steady-states may admit nonzero fluxes*. However, a phase-separated system with a planar interface will satisfy $\mathbf{j}^{\rho} = \mathbf{0}$ due to the quasi-1d geometry and no-flux boundary condition. We restrict our discussion to macroscopic phase separation. Therefore, both equilibrium and nonequilibrium systems will adopt a density flux-free state, reducing the linear momentum conservation to a static mechanical force balance:

$$\mathbf{0} = \boldsymbol{\nabla}\cdot\boldsymbol{\sigma} + \mathbf{b}. \quad \textbf{[4]}$$

*Phase-separated nonequilibrium systems with interfaces of finite curvature (i.e., if the domain of one of the coexisting phases is of nonmacroscopic spatial extent) may exhibit nonzero density fluxes (35).

Eq. **4** is the mechanical condition for liquid–gas coexistence and can be used to solve for $\rho(\mathbf{x})$ with constitutive equations for $\boldsymbol{\sigma}$ and $\mathbf{b}$. The nature of these constitutive equations will also determine whether other conservation equations will be required.

Let us now demonstrate that the equilibrium coexistence criteria are recovered from this mechanical perspective. In principle, for any system, whether it is in or out of equilibrium, microscopic expressions for Eqs. **2** and **3** can be obtained precisely through the N-body distribution function and its evolution equation. It will later be necessary to follow such an approach to obtain stresses and body forces when considering the phase coexistence of active particles. However, in equilibrium, the stresses and body forces can also be obtained variationally through a free energy functional. Consider the following free energy functional:

$$\mathcal{F}[\rho] = \int_V \left[f + \rho \mathcal{U}^{\text{ext}} + \frac{\kappa}{2} |\boldsymbol{\nabla}\rho|^2 \right] d\mathbf{x}, \qquad [5]$$

where $f(\rho)$ is the mean-field free energy density, $\kappa(\rho)$ is a (positive) coefficient such that the square-gradient term penalizes density gradients (36) and $\mathcal{U}^{\text{ext}}(\mathbf{x})$ represents all externally applied potential fields. Minimizing $\mathcal{F}[\rho]$ with respect to $\rho(\mathbf{x})$ (36–38) results, after some straightforward manipulations (*SI Appendix* for details), in Eq. **4**, allowing us to identify the reversible stress and body forces as

$$\boldsymbol{\sigma} = -p\mathbf{I} + \left(\frac{1}{2} \frac{\partial(\kappa\rho)}{\partial\rho} |\boldsymbol{\nabla}\rho|^2 + \kappa\rho\boldsymbol{\nabla}^2\rho \right) \mathbf{I} - \kappa \boldsymbol{\nabla}\rho\boldsymbol{\nabla}\rho, \quad [6a]$$

$$\mathbf{b} = -\rho\boldsymbol{\nabla}\mathcal{U}^{\text{ext}}, \qquad [6b]$$

where the pressure is again $p(\rho) = -f(\rho) + \rho\partial f/\partial\rho$ and $\mathbf{I}$ is the second-rank identity tensor. Note that the gradient terms appearing in Eq. **6a** are the so-called Korteweg stresses (39). The equilibrium coexistence criteria can now be obtained from Eqs. **4** and **6**.

Without loss of generality, we take the z-direction to be normal to the planar interface and neglect any external potential (i.e., $\mathbf{b} = \mathbf{0}$). In this case, the static force balance, Eq. **4** reduces to $d\sigma_{zz}/dz = 0$, where we have exploited the spatial invariance tangential to the interface. The stress is therefore constant across the interface resulting in

$$-\sigma_{zz} = p - \frac{1}{2}\left(\frac{\partial\kappa}{\partial\rho}\rho - \kappa \right) \left(\frac{d\rho}{dz} \right)^2 - \kappa\rho \frac{d^2\rho}{dz^2} = C, \qquad [7]$$

where C is a to-be-determined constant.

The complete density profile $\rho(z)$ can now be determined by solving Eq. **7** with the appropriate boundary conditions. For a macroscopically phase-separated system, the density profile approaches constant values ρ^{liq} and ρ^{gas} as $z \to \pm\infty$. In these regions of constant density, the gradient terms in Eq. **7** vanish and the pressure in the two phases is equal: $p(\rho^{\text{liq}}) = p(\rho^{\text{gas}}) = C$. We now recognize the constant C as the coexistence pressure p^{coexist} and recover the first of the two expected coexistence criteria in Eq. **1c**. Before proceeding to the second coexistence criteria, we rearrange Eq. **7**:

$$p(\rho) - p^{\text{coexist}} = a(\rho)\frac{d^2\rho}{dz^2} + b(\rho)\left(\frac{d\rho}{dz} \right)^2, \qquad [8]$$

where $a(\rho) = \kappa\rho$ and $b(\rho) = [(\partial\kappa/\partial\rho)\rho - \kappa]/2$. To recover the second coexistence criteria in a form similar to Eq. **1c**, we seek to integrate Eq. **8** with a variable such that the right-hand-side vanishes. Aifantis and Serrin (32) recognized that the gradient terms can be eliminated by multiplying Eq. **8** by a weighting function $E(\rho)d\rho/dz$, where

$$E(\rho) = \frac{1}{a(\rho)} \exp\left(2\int \frac{b(\rho)}{a(\rho)}\, d\rho \right), \qquad [9]$$

and spatially integrating the result across the interface. This operation eliminates the gradient terms, resulting in a coexistence criterion purely in terms of equations-of-state:

$$\int_{\rho^{\text{gas}}}^{\rho^{\text{liq}}} \left[p(\rho) - p^{\text{coexist}} \right] E(\rho)\, d\rho = 0. \qquad [10]$$

Aifantis and Serrin further established that Eq. **10** has a unique coexistence solution, provided $a(\rho) > 0$ and $p(\rho)$ is nonmonotonic in ρ (32).

Eq. **10** is no longer an equal-area construction, but such a form can be readily obtained through a simple change of variables (21, 22) $E(\rho) \equiv \partial\mathcal{E}/\partial\rho$ resulting in

$$\int_{\mathcal{E}^{\text{gas}}}^{\mathcal{E}^{\text{liq}}} \left[p(\mathcal{E}) - p^{\text{coexist}} \right] d\mathcal{E} = 0. \qquad [11]$$

Eq. **11** now has the form of an equal-area construction in the $p-\mathcal{E}$ plane. For the equilibrium system of interest, one finds that $E(\rho) = 1/\rho^2 = \upsilon^2$ and $\mathcal{E}(\rho) = \upsilon$ (multiplicative and additive constants in $E(\rho)$ and $\mathcal{E}(\rho)$ do not affect the coexistence criteria), recovering the expected equilibrium coexistence criteria, Eq. **1c** from our mechanical perspective.

We emphasize that, for equilibrium systems, retaining higher-order gradient terms in the free energy functional would not affect the resulting coexistence criteria, i.e., $\mathcal{E}(\rho) = \upsilon$ would remain the integration variable independent of the order of truncation. This can be verified by adding higher-order terms [e.g., ref. 40] to Eq. **5** (they must be even with respect to spatial gradients to satisfy the spatial inversion symmetry of the free energy) and confirming that, for the resulting stress, integration with respect to $\mathcal{E}(\rho) = \upsilon$ also eliminates the additional higher-order interfacial stress terms. This should not be surprising as, for equilibrium systems, the coexistence criteria can be derived without referencing the interface (as done at the beginning of this section) and thus should not depend on the precise details of the interface, including the truncation order.

We further note that in order to define the spinodal without invoking thermodynamic stability, a linear stability analysis on Eqs. **2** and **3** using the reversible stress Eq. **6a** can be performed to determine whether small density perturbations to a homogeneous base state will grow in time. In doing so (*SI Appendix* for details), we recover the mechanical spinodal criteria $(\partial p/\partial\rho) < 0$. This completes our discussion of the mechanics of equilibrium coexistence and stability.

For a nonequilibrium system, an additional complexity arises: the possibility of spontaneously generated internal body forces. The absence of applied external fields does not exclude the possibility of body forces for nonequilibrium systems. A general nonequilibrium coexistence criterion for liquid–gas phase separation must therefore account for these internal body forces. To understand this physically, let us consider a steady-state force balance on a collection of particles in a control volume Fig. 1. Application of an external force field on the particles results in a net volumetric force acting on the particles: a body force. By

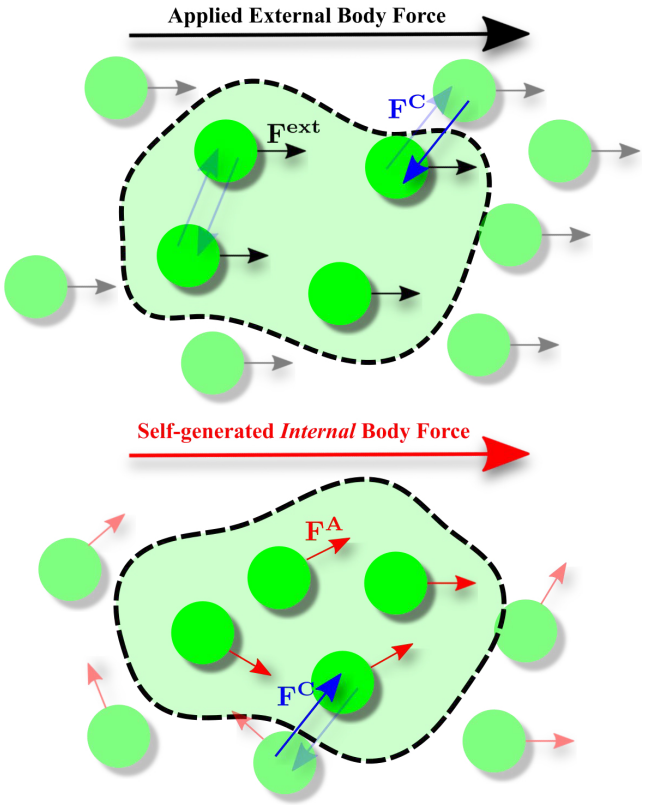

Fig. 1. Force balance on the particles within a control volume at steady state. Application of an external force field $\mathbf{F}^{\mathrm{ext}}$ (*Top*) to a passive system with conservative reciprocal interaction forces $\mathbf{F}^{\mathrm{C}}$ and a system with no external forces but with active forces $\mathbf{F}^{\mathrm{A}}$ in addition to $\mathbf{F}^{\mathrm{C}}$ (*Bottom*).

Newton's third law, interparticle interactions do not give rise to a net volumetric force within the volume interior. It is only at the surface of the control volume that interparticle forces (exerted by particles outside the volume on the interior particles) are nonvanishing, resulting in stresses. The polarization of active forces (*Bottom* of Fig. 1) results in a net active force within the volume, behaving similarly to an external force field (41).

At steady state, the self-generated body force density due to nonequilibrium forces must balance a stress difference across the volume. In this case, the steady-state one-dimensional (1d) mechanical balance is $d\sigma_{zz}/dz + b_z = 0$. For a one-dimensional system, the body force can always be expressed as $b_z = d\sigma^b/dz$, and the mechanical balance can now be expressed as $d(\sigma_{zz} + \sigma^b)/dz = 0$. This newly defined effective stress $\Sigma \equiv \sigma_{zz} + \sigma^b$ is, just as before, constant spatially. Expressing Σ as a second-order gradient expansion in density,

$$-\Sigma = \mathcal{P}(\rho) - a(\rho)\frac{d^2\rho}{dz^2} - b(\rho)\left(\frac{d\rho}{dz}\right)^2 = C, \qquad [12]$$

where $\mathcal{P}(\rho)$ is a dynamic or effective pressure. We again recognize that, as the gradients must vanish in the bulk phases, $\mathcal{P}(\rho^{\mathrm{liq}}) = \mathcal{P}(\rho^{\mathrm{gas}}) = C$, where we identify the constant as the coexistence effective pressure $\mathcal{P}^{\mathrm{coexist}}$. The second coexistence criteria can be found analogously as before through the use of an integrating factor $E(\rho)d\rho/dz$, where $E(\rho)$ is defined in Eq. **9**. The two coexistence criteria are then:

$$\mathcal{P}(\mathcal{E}^{\mathrm{liq}}) = \mathcal{P}(\mathcal{E}^{\mathrm{gas}}) = \mathcal{P}^{\mathrm{coexist}}, \qquad [13a]$$

$$\int_{\mathcal{E}^{\mathrm{gas}}}^{\mathcal{E}^{\mathrm{liq}}} \left[\mathcal{P}(\mathcal{E}) - \mathcal{P}^{\mathrm{coexist}}\right] d\mathcal{E} = 0, \qquad [13b]$$

where

$$\frac{\partial \mathcal{E}}{\partial \rho} = \frac{1}{a(\rho)} \exp\left(2\int \frac{b(\rho)}{a(\rho)}\, d\rho\right). \qquad [13c]$$

Eq. **13** is the general nonequilibrium coexistence criteria for liquid–gas phase separation.

The powerful idea that coexistence criteria can be extracted from knowledge of interfacial mechanics was, to the best of our knowledge, first proposed by Aifantis and Serrin (32) in the context of equilibrium systems. Solon and coworkers proposed a similar gradient-expansion-based approach beginning with a generalized Cahn–Hilliard model (21, 22). The criterion derived herein, Eq. **13** makes clear that for nonequilibrium phase separation, one criterion is always equality of dynamic pressure, while the other is obtained from knowledge of the interfacial stresses and body forces.

Application of this criterion to determine the phase diagram will require expressing the dynamic pressure $\mathcal{P}(\rho)$ as a second-order density gradient expansion in order to identify the equal-area construction variable $\mathcal{E}(\rho)$. Furthermore, provided that a timescale exists such that this dynamic pressure can also be defined for time-dependent states, the spinodal criterion is now $(\partial\mathcal{P}/\partial\rho) < 0$, as shown in *SI Appendix*. We now proceed to obtain the dynamic pressure of active Brownian particles and apply this nonequilibrium coexistence criterion.

The Mechanical Theory of MIPS

For a theoretical prediction of the phase diagram of active Brownian particles, our mechanical perspective requires expressions for the dynamic pressure, $\mathcal{P}(\rho)$, and the coefficients of the leading gradient terms, $a(\rho)$ and $b(\rho)$. These quantities are needed to calculate the appropriate integration variable $\mathcal{E}(\rho)$ such that Eq. **13** is satisfied. To derive these quantities, we require expressions for the stress $\boldsymbol{\sigma}$ and body forces $\mathbf{b}$ without invoking a variational principle. These constitutive equations can be obtained systematically, beginning with the equations-of-motion describing the motion of the microscopic degrees of freedom. We consider active Brownian particles with overdamped translational and rotational equations-of-motion describing the position $\mathbf{r}_\alpha$ and orientation $\mathbf{q}_\alpha$ ($|\mathbf{q}_\alpha| = 1$) of particle α as

$$\dot{\mathbf{r}}_\alpha = U_0\mathbf{q}_\alpha + \frac{1}{\zeta}\mathbf{F}^{\mathrm{C}}_\alpha, \qquad [14a]$$

$$\dot{\mathbf{q}}_\alpha = \boldsymbol{\Omega}^R_\alpha \times \mathbf{q}_\alpha, \qquad [14b]$$

where ζ is the translational drag coefficient and $\mathbf{F}^{\mathrm{C}}_\alpha$ is the interparticle force on particle α. The orientation of a particle evolves under the influence of a stochastic angular velocity $\boldsymbol{\Omega}^R_\alpha$, which follows the usual white noise statistics with a mean of $\langle\boldsymbol{\Omega}^R_\alpha(t)\rangle = \mathbf{0}$ and a variance of $\left\langle\boldsymbol{\Omega}^R_\alpha(t)\boldsymbol{\Omega}^R_\beta(t')\right\rangle = (2/\tau_R)\,\delta_{\alpha\beta}\delta(t-t')\mathbf{I}$, where τ_R is the reorientation time and $\delta_{\alpha\beta}$ is the Kronecker delta. We aim to describe the strongly active (athermal) limit of hard active disks and spheres where the phase diagram for these systems are fully described by two geometric parameters: the volume (or area) fraction $\phi \equiv v_p\rho$ (where v_p is the area ($d = 2$) or volume ($d = 3$) of a particle) and the dimensionless intrinsic run length ℓ_0/D, where $\ell_0 \equiv U_0\tau_R$, with D being the particle diameter and U_0 being the intrinsic active speed. We therefore choose a

conservative force $\mathbf{F}_\alpha^{\mathrm{C}}$ that results in hard-particle interactions, as further detailed in *Materials and Methods*.

The probability density $f_N(\mathbf{\Gamma};t)$ of finding the system in a microstate $\mathbf{\Gamma} = (\mathbf{r}^N, \mathbf{q}^N)$ at time t satisfies a conservation equation $\partial f_N/\partial t = \mathcal{L} f_N$, where $\mathcal{L}$ is the relevant dynamical operator specific to the microscopic equations-of-motion, e.g., Eq. **14**. Conservation equations needed to describe the density field (at a minimum, the continuity equation and linear momentum conservation) can be directly obtained through this dynamical operator and distribution function. For example, the continuity equation for the ensemble-averaged microscopic density $\rho(\mathbf{x};t) = \langle\hat{\rho}(\mathbf{x})\rangle = \left\langle\sum_{\alpha=1}^N \delta(\mathbf{x}-\mathbf{r}_\alpha)\right\rangle$ is given by $\partial\rho/\partial t = \int_\gamma \hat{\rho}\mathcal{L} f_N \, d\mathbf{\Gamma}$, where γ is the phase-space volume. An expression for linear momentum conservation and all other required conservation equations can be similarly obtained.

In the case of ABPs, $\mathcal{L}$ is the Fokker–Planck (or Smoluchowski) operator. For brevity, this operator and the conservation equations resulting from it are provided in *Materials and Methods*, and a complete derivation can be found in *SI Appendix*. Here, we include only the necessary results to obtain the MIPS phase diagram.

The linear momentum balance for overdamped ABPs is found to simply be $\mathbf{0} = \nabla\cdot\boldsymbol{\sigma} + \mathbf{b}$, where the inertial terms on the left-hand-side of Eq. **3** are identically zero. The stress is identified as $\boldsymbol{\sigma} = \boldsymbol{\sigma}^{\mathrm{C}}$, where $\boldsymbol{\sigma}^{\mathrm{C}}$ is the stress generated by the conservative interparticle forces. The body forces are given by $\mathbf{b} = -\zeta\mathbf{j}^\rho + \zeta U_0\mathbf{m}$, where $-\zeta\mathbf{j}^\rho$ is the drag force density and $\zeta U_0\mathbf{m}$ is the active force density arising from the polarization density field $\mathbf{m}(\mathbf{x};t) = \left\langle\sum_{\alpha=1}^N \mathbf{q}_\alpha\delta(\mathbf{x}-\mathbf{r}_\alpha)\right\rangle$. For the quasi-1d system, the active force density is the sole body force as $\mathbf{j}^\rho = \mathbf{0}$, reducing the linear momentum balance to

$$\mathbf{0} = \nabla\cdot\boldsymbol{\sigma}^{\mathrm{C}} + \zeta U_0\mathbf{m}. \qquad [15]$$

Activity thus manifests as a body force (41–44) rather than a true stress.

An added complexity for ABP coexistence is that we now require an additional conservation equation for the polarization density field $\mathbf{m}$ as it appears in Eq. **15**. This is given by

$$\mathbf{m} = -\frac{\tau_R}{d-1}\nabla\cdot\mathbf{j}^{\mathbf{m}}. \qquad [16]$$

The form of Eq. **16** allows us to write an *effective* stress for the system as

$$\mathbf{\Sigma} = \boldsymbol{\sigma}^{\mathrm{C}} + \boldsymbol{\sigma}^{\mathrm{act}}, \qquad [17]$$

where we have defined the active or "swim" (45) stress as $\boldsymbol{\sigma}^{\mathrm{act}} = -\zeta U_0\tau_R\mathbf{j}^{\mathbf{m}}/(d-1)$ (44). It is important to note here that the effective stress we define here is not a true stress just as the Maxwell stress tensor is not a true stress tensor (46). This distinction between true stresses ($\boldsymbol{\sigma}^{\mathrm{C}}$) and effective stresses ($\mathbf{\Sigma}$) was found to be crucial (44) in computing the surface tension of ABPs (47–49), which requires the true stress tensor (44, 50).

In our derivation of the effective stress, Eq. **17**, we have made no approximations. However, to utilize our nonequilibrium coexistence criteria, we must be able to express $\Sigma = \sigma_{zz}^{\mathrm{C}} + \sigma_{zz}^{\mathrm{act}}$ in terms of bulk equations-of-state and density gradients. A gradient expansion of the conservative interparticle stress σ_{zz}^C results in the bulk interaction pressure $p_{\mathrm{C}}(\rho)$ and Korteweg-like terms with coefficients related to the pair-interaction potential and pair-distribution function (38). In *SI Appendix*, we show the coefficients on the gradient terms associated with σ_{zz}^C scale as $\zeta U_0 D$—the stress scale for active hard-particle collisions—while, as we demonstrate next, the gradient terms in the active stress scale as $\zeta U_0\ell_0$. As MIPS occurs at $\ell_0/D \gg 1$, we can safely discard the Korteweg-like terms and approximate the conservative interparticle stress as $\sigma_{zz}^{\mathrm{C}} \approx -p_{\mathrm{C}}(\rho)$.

We now turn our focus to an expression for the active stress $\sigma_{zz}^{\mathrm{act}}$ in terms of bulk equations-of-state and density gradients. Deriving a constitutive equation for the polarization flux $\mathbf{j}^{\mathbf{m}}$ results in $\sigma_{zz}^{\mathrm{act}}$ taking the following form:

$$\sigma_{zz}^{\mathrm{act}}(z) = -\frac{\zeta\ell_0 U_0\overline{U}(\rho)}{d(d-1)}\left(\rho(z) + dQ_{zz}(z)\right), \qquad [18]$$

where Q_{zz} is the normal component of the traceless nematic density field $\mathbf{Q}(\mathbf{x};t) = \left\langle\sum_{\alpha=1}^N((\mathbf{q}_\alpha\mathbf{q}_\alpha - \mathbf{I}/d)\delta(\mathbf{x}-\mathbf{r}_\alpha)\right\rangle$. $U_0\overline{U}(\rho)$ is the density-dependent average speed of the particles. In the absence of interparticle interactions, the normalized speed $\overline{U}(\rho) = 1$ as particle motion is unencumbered. An equation-of-state for $\overline{U}(\rho)$ is required to describe this bulk contribution of the active stress. The nematic field satisfies its own conservation equation, which takes the following form at steady-state:

$$Q_{zz}(z) = -\frac{\tau_R}{2d}\frac{d}{dz}j_{zzz}^Q, \qquad [19a]$$

$$j_{zzz}^Q = U_0\overline{U}(\rho)B_{zzz}(z) + \left(\frac{3\overline{U}(\rho)}{d+2} - \frac{1}{d}\right)U_0 m_z(z) + \frac{1}{d\zeta}\frac{dp_{\mathrm{C}}}{dz}, \qquad [19b]$$

where B_{zzz} is the relevant component of the traceless third orientational moment $\mathbf{B} = \left\langle\sum_{\alpha=1}^N((\mathbf{q}_\alpha\mathbf{q}_\alpha\mathbf{q}_\alpha - \boldsymbol{\alpha}\cdot\mathbf{q}_\alpha/(d+2))\,\delta(\mathbf{x}-\mathbf{r}_\alpha)\right\rangle$, where $\boldsymbol{\alpha}$ is a fourth-rank isotropic tensor (*Materials and Methods* or *SI Appendix*). As we are interested in density gradients up to second order, we can safely close the hierarchy of orientational moments by setting $\mathbf{B} = \mathbf{0}$. We also recognize from linear momentum conservation Eq. **15** that $\zeta U_0 m_z - dp_{\mathrm{C}}/dz = 0$, allowing us to substitute p_{C} in place of m_z in Eq. **19b**. Our expression for the effective stress is now:

$$-\Sigma = p_{\mathrm{C}} + p_{\mathrm{act}} - \frac{3\ell_0^2}{2d(d-1)(d+2)}\overline{U}(\rho)\frac{d}{dz}\left(\overline{U}(\rho)\frac{dp_{\mathrm{C}}}{dz}\right), \qquad [20]$$

where $p_{\mathrm{act}} = \rho\zeta\ell_0 U_0\overline{U}(\rho)/d(d-1)$ is the active pressure (43–45, 51–54)—an effective pressure emerging from the active body force density.

The mechanical terms needed to apply our nonequilibrium coexistence criteria, for a given activity ℓ_0, can now be identified as

$$\mathcal{P}(\rho) = p_{\mathrm{C}} + p_{\mathrm{act}}, \qquad [21a]$$

$$a(\rho) = \frac{3\ell_0^2}{2d(d-1)(d+2)}\overline{U}^2\frac{\partial p_{\mathrm{C}}}{\partial\rho}. \qquad [21b]$$

$$b(\rho) = \frac{3\ell_0^2}{2d(d-1)(d+2)}\overline{U}\frac{\partial}{\partial\rho}\left[\overline{U}\frac{\partial p_{\mathrm{C}}}{\partial\rho}\right], \qquad [21c]$$

Eqs. **13c**, **21a**, and **21b** allow us to identify $\mathcal{E}(\rho) = p_{\mathrm{C}}(\rho)$. The coexistence criteria for MIPS is therefore

$$\mathcal{P}(p_{\mathrm{C}}^{\mathrm{liq}}) = \mathcal{P}(p_{\mathrm{C}}^{\mathrm{gas}}) = \mathcal{P}^{\mathrm{coexist}}, \qquad [22a]$$

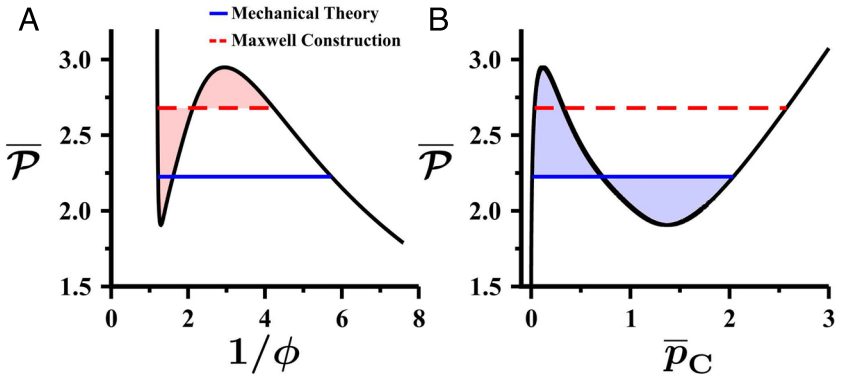

Fig. 2. Predicted homogeneous equation-of-state for 2d athermal ABPs (61) with $\ell_0/D \approx 31.2$. (*A*) The equal-area Maxwell construction in the $\mathcal{P} - \phi^{-1}$ plane overestimates the coexistence pressure as predicted from (*B*) the equal-area construction in $\mathcal{P} - p_C$ established by our nonequilibrium theory. $\mathcal{P}$ and p_C are made dimensionless by $\zeta U_0 D/v_p$.

$$\int_{p_C^{gas}}^{p_C^{liq}} \left[\mathcal{P}(p_C) - \mathcal{P}^{coexist}\right] dp_C = 0. \qquad [22b]$$

Furthermore, the spinodal criterion is indeed found to be $(\partial\mathcal{P}/\partial\rho) < 0$ (*SI Appendix* for details).

To apply this coexistence criterion, we need to know the functional form of $p_C(\rho, \ell_0)$ and $p_{act}(\rho, \ell_0)$ (or equivalently $\overline{U}$) as a function of volume fraction ϕ (in place of ρ) and activity ℓ_0/D. A detailed theoretical treatment for these equations-of-state will require a theory for the pair-distribution function $g(\mathbf{r}, \mathbf{q})$ where $\mathbf{r}$ and $\mathbf{q}$ are the separation vector and relative orientation vector between particle pairs, respectively. The description of nonequilibrium pair-correlations is an active area of investigation. Theories applicable in the dilute limit have been proposed (55), and recent developments have been made toward our understanding of strongly interacting systems (56, 57). Closure relations rooted in ideas from dynamical density functional theory (58) have also been proposed for a variety of active systems, including ABPs (24, 49), hydrodynamically interacting microswimmers (59), and active rods (60), to name a few.

An alternative approach is to obtain these equations-of-state directly from particle-based simulations in regions of the $\phi - \ell_0$ plane where the system remains homogeneous. This measured behavior can then be extrapolated to regions of the $\phi - \ell_0$ plane where the equations-of-state cannot be directly obtained by leveraging a number of physical considerations (e.g., p_C is a monotonically increasing function of both ϕ and ℓ_0), as detailed in ref. 61. In two dimensions (2d), we utilize the equations-of-state developed in ref. 61 and follow a similar procedure to develop three-dimensional (3d) versions, provided in *SI Appendix*. We note that in both 2d (62) and 3d (63), ABPs can exhibit an order-disorder transition. The theory presented here applies only to scenarios where the sole order parameter is density. We therefore limit our focus to polydisperse ABPs in 2d (eliminating any potential ordered phase) and, in 3d, recognize that the liquid–gas transition is metastable with respect to a fluid–crystal transition for much of the phase diagram (63).

Fig. 2 compares the results of performing the equal-area construction in the $\mathcal{P} - p_C$ plane with the naive application of the Maxwell (equilibrium) equal-area-construction in the $\mathcal{P} - \upsilon$ plane (where $\upsilon \sim 1/\phi$). The equilibrium construction overestimates the coexistence pressure in comparison to our nonequilibrium theory, resulting in less disparate coexisting densities. This trend holds in both two and three dimensions (binodals presented in Fig. 3) and is exacerbated with increasing activity.

We now compare our theory with extensive simulations of polydisperse hard disks (2d) performed in this study, Fig. 3*A* and simulations of monodisperse hard spheres (3d) conducted in ref. 63, Fig. 3*B*. The agreement between our theory and

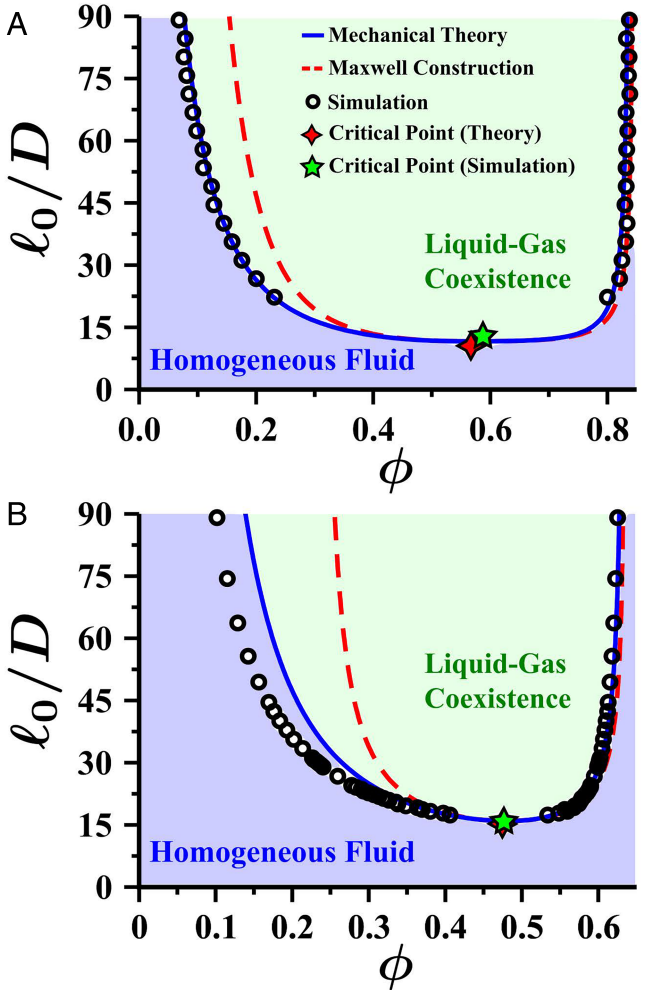

Fig. 3. Coexistence curves for athermal active Brownian (*A*) disks (2d) and (*B*) spheres (3d). Coexisting densities were obtained from slab simulation data collected in this work (2d) and from ref. 63 (3d). Critical points displayed were estimated from simulations in refs. 64 (2d) and (63) (3d). Regions of coexistence and homogeneity are shaded on the basis of our theoretical predictions.

simulation data is nearly perfect in 2d and, while there is less agreement in 3d, the nonequilibrium theory provides a substantially improved binodal in comparison to that predicted by the equilibrium Maxwell construction. We note that, just as in equilibrium theories for coexistence, the quantitative accuracy of any theory for nonequilibrium coexistence will of course depend on the quality of the equations-of-state, a potential source of the discrepancy in 3d.

Nonequilibrium Interfacial Phenomena

At this point, let us now consider physically why our nonequilibrium mechanical theory consistently predicts a wider binodal when compared to the equilibrium Maxwell construction in the $p-\upsilon$ plane. We first note that Eq. **1c** has a clear mechanical interpretation. The integrand $p(\upsilon)-p^{\text{coexist}}$ isolates the contribution to the pressure arising solely due to interfacial forces. The integral can thus be interpreted as the mechanical work exerted by the interfacial forces on a particle as it moves from one phase to the other. In equilibrium, this (reversible) work is identically zero: Moving a particle from liquid to gas (or gas to liquid) requires no work. In the case of ABPs, performing the equilibrium Maxwell construction in the $p-\upsilon$ plane with the coexistence pressure $\mathcal{P}^{\text{coexist}}$ determined from the nonequilibrium theory, Fig. 2*A*, the interface works against particle removal from the liquid phase:

$$\mathcal{W}_{\text{interf}}^{\text{liq}\to\text{gas}}=\int_{\upsilon^{\text{liq}}}^{\upsilon^{\text{gas}}}\left[\mathcal{P}(\upsilon)-\mathcal{P}^{\text{coexist}}\right]\,d\upsilon\geq 0, \qquad [23]$$

where the equality holds only at the critical point. This physical picture is consistent with the unique interfacial structure of MIPS, where ABPs within the interface are polarized facing into the liquid phase. As activity increases, this interfacial polarization intensifies and so, too, does the departure from the equilibrium Maxwell construction.

The above discussion makes clear that nonequilibrium interfacial forces play a determining role in the phase behavior of driven systems. We can investigate this interfacial structure in greater detail as our mechanical theory, by its very nature, makes predictions about the structure of the interface that can be compared with simulation. We emphasize that, just as is the case for equilibrium systems, a small gradient theory may fail to quantitatively capture the precise structure of the interface while accurately describing the binodal. A solution of Eq. **20** is shown in Fig. 4, where we find good qualitative agreement between our mechanical theory and simulation results for the density ϕ, polarization m_z, and nematic order Q_{zz} profiles. Additionally, we observe that the polar order is proportional to $d\phi/dz$, and the nematic order is proportional to dm_z/dz, as predicted by their conservation equations.

The polarization density, implicated above in the violation of the equilibrium Maxwell construction, can be understood as follows. From the momentum balance, the difference in p_{C} between the two phases is balanced by the integral of the active force density: $p_{\text{C}}(\rho^{\text{liq}})-p_{\text{C}}(\rho^{\text{gas}})=\int_{z^{\text{gas}}}^{z^{\text{liq}}}\zeta U_0 m_z dz$. Particles at the interface are oriented and exert active forces toward the phase with a higher interaction pressures or density, suppressing the removal of particles from the liquid phase. In the absence of these interfacial active forces (and in the absence of attractive cohesive forces keeping the liquid intact), there would be nothing to prevent the complete dissolution of the liquid phase.

The internally generated active force density engenders a unique nonmonotonic trend in the interfacial width (*Materials and Methods*), predicted by our theory (Fig. 5). This behavior was first observed in the simulations of Lauersdorf et al. (50) and reproduced here in our simulations of active spheres (Fig. 5, *Inset*). This trend is in stark contrast to interfaces in equilibrium

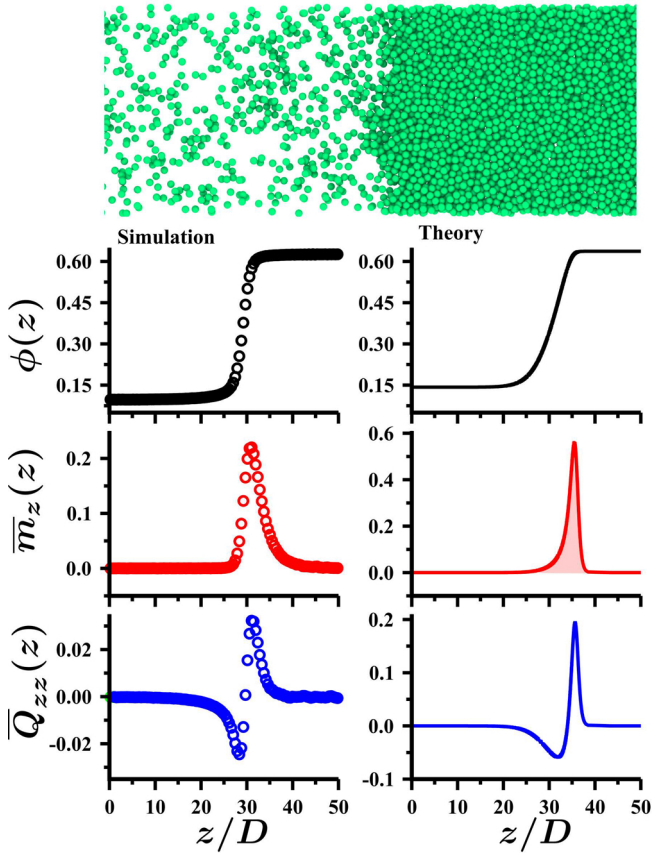

Fig. 4. Comparison of the one-body orientational moments obtained from simulation and theory for 3d ABPs with $\ell_0/D\approx 44.5$. Snapshot represents an instantaneous system configuration. Only a narrow slice (in the out-of-plane direction) of particles is shown for clarity. Polar and nematic order profiles are made dimensionless by the particle volume. Spatial integral of m_z (shaded) is directly proportional to the difference in liquid and gas phase pressures, coupling the interfacial structure to the bulk phase behavior.

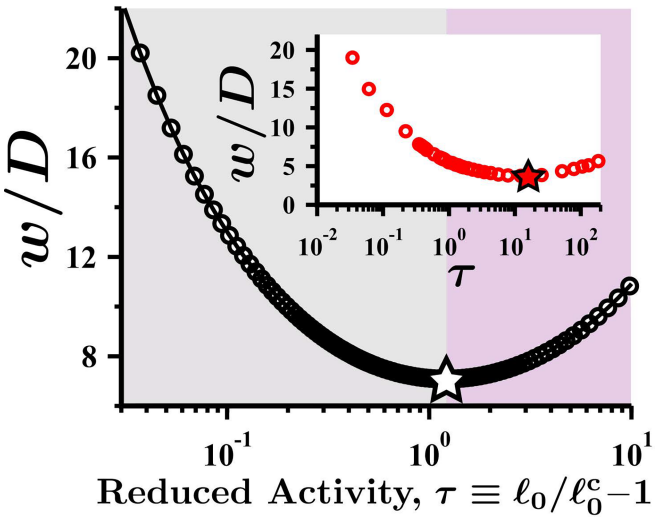

Fig. 5. Theoretical interfacial width w of 3d ABPs as a function of the critical parameter (where ℓ_0^{c} is the critical activity) with simulations (*Inset*) corroborating the predicted nonmonotonicity. Stars denote local minima.

systems where the width of the interface decreases monotonically as the system is taken deeper into the coexistence region. Again, while a small gradient theory is not expected to quantitatively capture the structure of the interface, our theory is able to capture this effect qualitatively.

To illustrate that the origins of this unique nonequilibrium effect are again rooted in the interfacial active force density, consider the following. As one moves deeper into the two-phase region, the difference in interaction pressures (or densities) between coexisting phases increases and so must the total active force provided by the particles at the interface to maintain this density difference. For sufficiently low activities, the active force required can be achieved by amplifying the active force density, $\zeta U_0 m_z = \zeta U_0 \rho \langle q_z \rangle$, by better alignment of particle orientations $\langle q_z \rangle$ toward the liquid phase, which results in a more compact and thinner interface. However, this reinforcement mode is limited due to the upper bound of the magnitude of the active force density imposed by perfect alignment $\langle q_z \rangle = 1$. To supply the large required active force needed at high activity, the width of the interface must increase with activity—once a packed layer of particles is fully aligned, more layers are necessary to produce the required active force.

Discussion and Conclusions

The nonequilibrium mechanical theory presented in this work allows for the determination of phase diagrams from bulk equations-of-state without making any assumptions regarding the distribution of microstates. Our theory identifies the effective pressure $\mathcal{P}$, which includes the pressure arising from conservative interactions and those arising from nonequilibrium body forces, as the critical mechanical quantity in determining the phase behavior of nonequilibrium systems. Using MIPS as a case study, we find that using a true nonequilibrium coexistence theory results in significantly better predictions than the binodal obtained through the naive use of the equilibrium coexistence criteria.

In equilibrium, the coexistence criteria for phase separation are independent of the system details. All that is required is the equation-of-state (the pressure or chemical potential) to determine the phase diagram. For nonequilibrium systems, the interfacial stresses must be determined to derive the coexistence criteria, which will generally result in system-specific coexistence criteria [i.e., a system specific $\mathcal{E}(\rho)$]. Moreover, while the order at which the density-gradient expansion is truncated for equilibrium systems will not affect $\mathcal{E}(\rho)$, there is no such guarantee for nonequilibrium systems. This is a result of the coefficients for a nonequilibrium system generally not emerging from a variational principle as in equilibrium. These considerations might suggest that the equilibrium coexistence criteria, while both rigorously and quantitatively incorrect, might at least provide a rough pragmatic estimate for the binodal of a nonequilibrium material (19, 34). However, any departure from the equilibrium Maxwell construction likely indicates the significance of nonequilibrium interfacial forces. Indeed, our theory reveals that the internally generated active force density—present only within the interface—dictates the interface's structure and, in turn, the appropriate coexistence criteria.

Finally, the mechanical theory for nonequilibrium phase separation presented in this work applies to scenarios where density is the sole order parameter. A myriad of other nonequilibrium phase transitions have been observed in recent years, including symmetry-breaking transitions [such as active crystallization (63)], transitions with nonconserved order parameters (14), and transitions with multiple order parameters, including traveling states (65–68). A general mechanical theory, such as that developed here, for these and other phase transitions would provide a much-needed framework for constructing and characterizing nonequilibrium coexistence.

Materials and Methods

Here, we briefly summarize the simulation and theoretical details, while a detailed derivation of the ABP conservation equations is provided in *SI Appendix*.

Simulations. Particle-based simulations were conducted to determine the binodal for 2d polydisperse disks equations-of-state for this system were exhaustively determined in ref. 61 and the equations-of-state for monodisperse 3d hard spheres the binodal of this system was determined in ref. 63. In all simulations, particles follow the equations-of-motion provided in the main text, Eqs. **14a** and **14b**, and the interparticle force $\mathbf{F}^{\mathsf{C}}[\mathbf{r}^N; \varepsilon, \sigma]$ is taken to result from a Weeks–Chandler–Anderson (WCA) potential (69) (characterized by a Lennard-Jones diameter σ_{LJ} and energy scale ε). Despite the use of a continuous potential, hard-particle statistics can be effectively achieved through careful consideration of the different force scales, as discussed in ref. 63. Lacking translational Brownian motion, which simply attenuates the influence of activity on the phase behavior, these particles strictly exclude volume with a diameter D set by the potential stiffness $\mathcal{S} \equiv \varepsilon/(\zeta U_0 \sigma_{\mathsf{LJ}})$ as a measure of the relative strength of conservative and active forces. Continuous repulsions act only at distances between D and $2^{1/6}\sigma_{\mathsf{LJ}}$, a range that quickly becomes negligible as the stiffness $\mathcal{S}$ increases. We use a stiffness $\mathcal{S} = 50$ for which $D/(2^{1/6}\sigma_{\mathsf{LJ}}) = 0.9997$, effectively achieving hard-sphere statistics. We therefore take the diameter to simply be $D = 2^{1/6}\sigma_{\mathsf{LJ}}$. Holding $\mathcal{S}$ fixed to remain in this hard-sphere limit, the system state is independent of the active force magnitude and is fully described by two geometric parameters: the volume fraction $\phi = N\pi D^3/6V$ (or area fraction $\phi = N\pi D^2/4A$) and the dimensionless intrinsic run length ℓ_0/D.

All simulations were conducted with a minimum of 54,000 particles using the GPU-enabled HOOMD-blue software package (70). Additional details for the construction of the 3d equations-of-state are provided in *SI Appendix*.

Fokker–Planck Equation. The Fokker–Planck (or Smoluchowski) describing the N-body distribution of particle positions and orientations has the following form:

$$\frac{\partial f_N}{\partial t} + \sum_\alpha \nabla_\alpha \cdot \mathbf{j}_\alpha^T + \sum_\alpha \nabla_\alpha^R \cdot \mathbf{j}_\alpha^R = 0. \qquad [24a]$$

Here, $f_N(\Gamma, t)$ is the probability density of observing a configuration $\Gamma \equiv (\mathbf{r}_1, \mathbf{r}_2, ..., \mathbf{r}_N, \mathbf{q}_1, \mathbf{q}_2, ..., \mathbf{q}_N)$ at time t, $\mathbf{r}_\alpha$ and $\mathbf{q}_\alpha$ ($|\mathbf{q}_\alpha| = 1$) are the position and orientation vectors of particle α, $\mathbf{j}_\alpha^T$ and $\mathbf{j}_\alpha^R$ are translational and rotational fluxes of particle α, and $\nabla_\alpha = \partial/\partial \mathbf{r}_\alpha$ and $\nabla_\alpha^R = \mathbf{q}_\alpha \times \partial/\partial \mathbf{q}_\alpha$ are translational and rotational gradient operators. The fluxes are given by

$$\mathbf{j}_\alpha^T = U_0 \mathbf{q}_\alpha f_N + \frac{1}{\zeta}\mathbf{F}_\alpha^{\mathsf{C}} f_N, \qquad [24b]$$

$$\mathbf{j}_\alpha^R = -\tau_R^{-1} \nabla_\alpha^R f_N. \qquad [24c]$$

The application of our nonequilibrium coexistence theory requires the steady-state (and density flux-free) linear momentum balance and the conservation equations of any field variable appearing in the momentum balance. Eq. **24** and the microscopic definition of the field variables can be used to obtain these conservation equations (*SI Appendix* for details), which are summarized next.

Conservation Equations. Conservation of number density is simply the continuity equation:

$$\frac{\partial \rho}{\partial t} + \nabla \cdot \mathbf{j}^\rho = 0, \qquad [25]$$

which is coupled to linear momentum conservation:

$$\mathbf{0} = \nabla \cdot \boldsymbol{\sigma}^{\mathsf{C}} + \zeta U_0 \mathbf{m} - \zeta \mathbf{j}^\rho. \qquad [26]$$

The polar order field $\mathbf{m}(\mathbf{x}, t)$ satisfies its own conservation equation:

$$\frac{\partial \mathbf{m}}{\partial t} + \nabla \cdot \mathbf{j}^{\mathbf{m}} + \frac{d-1}{\tau_R}\mathbf{m} = \mathbf{0}, \qquad [27a]$$

where the polarization flux follows:

$$\mathbf{j}^{\mathbf{m}} = U_0 \overline{U}\left(\mathbf{Q} + \frac{1}{d}\rho \mathbf{I}\right). \qquad [27b]$$

A microscopic expression for the dimensionless average active speed $\overline{U}$ is provided in *SI Appendix*. An additional term, not included in Eq. **27b**, also appears but is found to have only a negligible quantitative effect on our findings as detailed in *SI Appendix*.

The nematic order conservation and constitutive equations are found to be

$$\frac{\partial \mathbf{Q}}{\partial t} + \nabla \cdot \mathbf{j}^{\mathbf{Q}} + \frac{2d}{\tau_R}\mathbf{Q} = \mathbf{0}, \qquad [28a]$$

$$\mathbf{j}^{\mathbf{Q}} = U_0 \overline{U}\mathbf{B} + U_0 \mathbf{m} \cdot \left(\frac{\overline{U}}{d+2}\boldsymbol{\alpha} - \frac{1}{d}\mathbf{II}\right) - \frac{1}{d\zeta}\nabla \cdot \boldsymbol{\sigma}^{\mathrm{C}}\mathbf{I}, \qquad [28b]$$

where $\boldsymbol{\alpha}$ is an isotropic fourth-rank tensor. (In indicial notation, $\alpha_{ijkl} = \delta_{ij}\delta_{kl} + \delta_{ik}\delta_{jl} + \delta_{il}\delta_{jk}$, where δ_{ij} is the second-rank identity tensor.) In Eq. **28b**, the microscopic expression for $\overline{U}$ differs from that in Eq. **27b**. However, to good approximation, these speeds can be taken to be the same, allowing us to express the steady-state equations with only two equations-of-state: p_{C} and $\overline{U}$.

Interfacial Width Definition. The interfacial width is not a uniquely defined quantity. Here, for both our theory and simulations, we compute the interfacial width using the ensemble-averaged density profile, $\phi(z)$. We seek a definition of interfacial width which does not presume a particular functional form of $\phi(z)$. We therefore use the "10-90 thickness" (71) definition of interfacial width, which defines the width as the distance between the two locations, z_1 and z_2 (i.e., $w = |z_2 - z_1|$), at which $\phi(z_1) = \phi^{\mathrm{gas}} + 0.1(\phi^{\mathrm{liq}} - \phi^{\mathrm{gas}})$ and $\phi(z_2) = \phi^{\mathrm{gas}} + 0.9(\phi^{\mathrm{liq}} - \phi^{\mathrm{gas}})$. The qualitative results were found to be insensitive to the precise definition of interfacial width.

Data, Materials, and Software Availability. All study data are included in the article and/or *SI Appendix*.

ACKNOWLEDGMENTS. A.K.O. is deeply indebted to Phill Geissler for his numerous insights regarding this work. We thank Katie Klymko, Karol Makuch, Yizhi Shen, Zhiwei Peng, Andy Ylitalo, Dan Evans, and Luke Langford for helpful discussions. We gratefully acknowledge support from the Schmidt Science Fellowship in partnership with the Rhodes Trust (A.K.O.), Kwanjeong Educational Foundation (H.R.), Arnold and Mabel Beckman Foundation (S.A.M.), and NSF under grant no. CBET-1803662 (J.F.B.).

Author affiliations: [a]Department of Materials Science and Engineering, University of California, Berkeley, CA 94720; [b]Materials Sciences Division, Lawrence Berkeley National Laboratory, Berkeley, CA 94720; [c]Division of Chemistry and Chemical Engineering, California Institute of Technology, Pasadena, CA 91125; and [d]Department of Chemistry, The Pennsylvania State University, University Park, PA 16802

1. J. Berry, C. P. Brangwynne, M. Haataja, Physical principles of intracellular organization via active and passive phase transitions (2018).
2. C. F. Lee, Formation of liquid-like cellular organelles depends on their composition (2020).
3. A. Radja, E. M. Horsley, M. O. Lavrentovich, A. M. Sweeney, Pollen cell wall patterns form from modulated phases correspondence in brief a biophysical model explains the non-equilibrium phase-separation properties in polysaccharides that form distinct, characteristic patterns on the surface of pollen grains across the diversity of plants. *Cell* **176**, 856–868 (2019).
4. R. Besseling *et al.*, Shear banding and flow-concentration coupling in colloidal glasses. *Phys. Rev. Lett.* **105**, 268301 (2010).
5. H. Eugene, G. Fredrickson, Large fluctuations in polymer solutions under shear. *Phys. Rev. Lett.* **62**, 2468–2471 (1989).
6. S. M. Fielding, P. D. Olmsted, Flow phase diagrams for concentration-coupled shear banding. *Euro. Phys. J. E* **11**, 65–83 (2003).
7. M. E. Helgeson, L. Porcar, C. Lopez-Barron, N. J. Wagner, Direct observation of flow-concentration coupling in a shear-banding fluid. *Phys. Rev. Lett.* **105**, 084501 (2010).
8. A. K. Omar, Z. G. Wang, Shear-induced heterogeneity in associating polymer gels: Role of network structure and dilatancy. *Phys. Rev. Lett.* **119**, 117801 (2017).
9. M. E. Cates, J. Tailleur, Motility-induced phase separation. *Annu. Rev. Condens. Matter Phys.* **6**, 219–244 (2015).
10. A. V. Ivlev *et al.*, Statistical mechanics where newton's third law is broken. *Phys. Rev. X* **5**, 011035 (2015).
11. K. Klymko, P. L. Geissler, S. Whitelam, Microscopic origin and macroscopic implications of lane formation in mixtures of oppositely driven particles. *Phys. Rev. E* **94**, 022608 (2016).
12. M. Han, J. Yan, S. Granick, E. Luijten, Effective temperature concept evaluated in an active colloid mixture. *Proc. Natl. Acad. Sci. U.S.A.* **114**, 7513–7518 (2017).
13. C. del Junco, L. Tociu, S. Vaikuntanathan, Energy dissipation and fluctuations in a driven liquid. *Proc. Natl. Acad. Sci. U.S.A.* **115**, 3569–3574 (2018).
14. M. Fruchart, R. Hanai, P. B. Littlewood, V. Vitelli, Non-reciprocal phase transitions. *Nature* **592**, 363 (2020).
15. J. Clerk-Maxwell, On the dynamical evidence of the molecular constitution of bodies. *Nature* **11**, 357–359 (1875).
16. Y. Fily, M. C. Marchetti, Athermal phase separation of self-propelled particles with no alignment. *Phys. Rev. Lett.* **108**, 235702 (2012).
17. G. S. Redner, M. F. Hagan, A. Baskaran, Structure and dynamics of a phase-separating active colloidal fluid. *Phys. Rev. Lett.* **110**, 055701 (2013).
18. R. Wittkowski *et al.*, Scalar ϕ 4 field theory for active-particle phase separation. *Nat. Commun.* **5**, 4351 (2014).
19. S. C. Takatori, J. F. Brady, Towards a thermodynamics of active matter. *Phys. Rev. E* **91**, 032117 (2015).
20. S. Chakraborti, S. Mishra, P. Pradhan, Additivity, density fluctuations, and nonequilibrium thermodynamics for active Brownian particles. *Phys. Rev. E* **93**, 052606 (2016).
21. A. P. Solon, J. Stenhammar, M. E. Cates, Y. Kafri, J. Tailleur, Generalized thermodynamics of motility-induced phase separation: Phase equilibria, Laplace pressure, and change of ensembles. *New J. Phys.* **20**, 75001 (2018).
22. A. P. Solon, J. Stenhammar, M. E. Cates, Y. Kafri, J. Tailleur, Generalized thermodynamics of phase equilibria in scalar active matter. *Phys. Rev. E* **97**, 020602(R) (2018).
23. S. Paliwal, J. Rodenburg, R. v. Roij, M. Dijkstra, Chemical potential in active systems: Predicting phase equilibrium from bulk equations of state? *New J. Phys.* **20**, 015003 (2018).
24. S. Hermann, P. Krinninger, D. de las Heras, M. Schmidt, Phase coexistence of active Brownian particles. *Phys. Rev. E* **100**, 52604 (2019).
25. S. Hermann, D. de las Heras, M. Schmidt, Phase separation of active Brownian particles in two dimensions: Anything for a quiet life. *Mol. Phys.* **119**, e1902585 (2021).
26. T. Speck, Coexistence of active Brownian disks: Van der Waals theory and analytical results. *Phys. Rev. E* **103**, 12607 (2021).
27. G. S. Redner, C. G. Wagner, A. Baskaran, M. F. Hagan, Classical nucleation theory description of active colloid assembly. *Phys. Rev. Lett.* **117**, 148002 (2016).
28. T. Speck, J. Bialké, A. M. Menzel, H. Löwen, Effective Cahn-Hilliard equation for the phase separation of active Brownian particles. *Phys. Rev. Lett.* **112**, 218304 (2014).
29. S. Whitelam, K. Klymko, D. Mandal, Phase separation and large deviations of lattice active matter. *J. Chem. Phys.* **148**, 154902 (2018).
30. T. GrandPre, K. Klymko, K. K. Mandadapu, D. T. Limmer, Entropy production fluctuations encode collective behavior in active matter. *Phys. Rev. E* **103**, 012613 (2021).
31. H. T. Davis, L. E. Scriven, "Stress and structure in fluid interfaces" in *Advances Chemical Physics* (John Wiley & Sons, Ltd., 1982), pp. 357–454.
32. E. C. Aifantis, J. B. Serrin, Equilibrium solutions in the mechanical theory of fluid microstructures. *J. Colloid Interf. Sci.* **96**, 530–547 (1983).
33. E. C. Aifantis, J. B. Serrin, The mechanical theory of fluid interfaces and Maxwell's rule. *J. Colloid Interf. Sci.* **96**, 517–529 (1983).
34. J. Zhang, R. Alert, J. Yan, N. S. Wingreen, S. Granick, Active phase separation by turning towards regions of higher density. *Nat. Phys.* **17**, 961–967 (2021).
35. E. Tjhung, C. Nardini, M. E. Cates, Cluster phases and bubbly phase separation in active fluids: Reversal of the Ostwald process. *Phys. Rev. X* **8**, 031080 (2018).
36. J. W. Cahn, J. E. Hilliard, Free energy of a nonuniform system. I. Interfacial free energy. *J. Chem. Phys.* **28**, 258–267 (1958).
37. J. D. der Waals, *Thermodynamische theorie der capillariteit in de onderstelling van continue dichtheidsverandering* (Verhand. Kon. Akad. Wetensch, Amsterdam Sect, 1893), p. 1.
38. A. J. M. Yang, P. D. Fleming, J. H. Gibbs, Molecular theory of surface tension. *J. Chem. Phys.* **64**, 3732–3747 (1976).
39. D. J. Korteweg, Archives neerl. *Sci. Exacts. Nat.* **6** (1904).
40. B. Z. Shang, N. K. Voulgarakis, J. W. Chu, Fluctuating hydrodynamics for multiscale simulation of inhomogeneous fluids: Mapping all-atom molecular dynamics to capillary waves. *J. Chem. Phys.* **135**, 044111 (2011).
41. W. Yan, J. F. Brady, The swim force as a body force. *Soft Matter* **11**, 6235–6244 (2015).
42. J. Rodenburg, M. Dijkstra, R. Van Roij, Van't Hoff's law for active suspensions: The role of the solvent chemical potential. *Soft Matter* **13**, 8957–8963 (2017).
43. J. M. Epstein, K. Klymko, K. K. Mandadapu, Statistical mechanics of transport processes in active fluids. II. Equations of hydrodynamics for active Brownian particles. *J. Chem. Phys.* **150**, 164111 (2019).
44. A. K. Omar, Z. G. Wang, J. F. Brady, Microscopic origins of the swim pressure and the anomalous surface tension of active matter. *Phys. Rev. E* **101**, 012604 (2020).
45. S. C. Takatori, W. Yan, J. F. Brady, Swim pressure: Stress generation in active matter. *Phys. Rev. Lett.* **113**, 028103 (2014).
46. C. Rinaldi, H. Brenner, Body versus surface forces in continuum mechanics: Is the Maxwell stress tensor a physically objective Cauchy stress? *Phys. Rev. E* **65**, 036615 (2002).
47. J. Bialké, J. T. Siebert, H. Löwen, T. Speck, Negative interfacial tension in phase-separated active Brownian particles. *Phys. Rev. Lett.* **115**, 98301 (2015).

48. A. Patch, D. M. Sussman, D. Yllanes, M. C. Marchetti, Curvature-dependent tension and tangential flows at the interface of motility-induced phases. *Soft Matter* **14**, 7435–7445 (2018).
49. S. Hermann, Heras D. De Las, M. Schmidt, Non-negative interfacial tension in phase-separated active Brownian particles. *Phys. Rev. Lett.* **123**, 268002 (2019).
50. N. Lauersdorf, T. Kolb, M. Moradi, E. Nazockdast, D. Klotsa, Phase behavior and surface tension of soft active Brownian particles. *Soft Matter* **17**, 6337–6351 (2021).
51. Y. Fily, S. Henkes, M. C. Marchetti, Freezing and phase separation of self-propelled disks. *Soft Matter* **10**, 2132–2140 (2014).
52. S. A. Mallory, A. Šarić, C. Valeriani, A. Cacciuto, Anomalous thermomechanical properties of a self-propelled colloidal fluid. *Phys. Rev. E* **89**, 052303 (2014).
53. A. P. Solon *et al*., Pressure and phase equilibria in interacting active Brownian spheres. *Phys. Rev. Lett.* **114**, 198301 (2015).
54. A. P. Solon *et al*., Pressure is not a state function for generic active fluids. *Nat. Phys.* **11**, 673–678 (2015).
55. T. M. Squires, J. F. Brady, A simple paradigm for active and nonlinear microrheology. *Phys. Fluids* **17**, 73101 (2005).
56. L. Tociu, É. Fodor, T. Nemoto, S. Vaikuntanathan, How dissipation constrains fluctuations in nonequilibrium liquids: Diffusion, structure, and biased interactions. *Phys. Rev. X* **9**, 041026 (2019).
57. L. Tociu, G. Rassolov, É. Fodor, S. Vaikuntanathan, Mean-field theory for the structure of strongly interacting active liquids. *J. Chem. Phys.* **157**, 014902 (2022).
58. M. te Vrugt, H. Löwen, R. Wittkowski, Classical dynamical density functional theory: From fundamentals to applications. *Adv. Phys.* **69**, 121–247 (2020).
59. A. M. Menzel, A. Saha, C. Hoell, H. Löwen, Dynamical density functional theory for microswimmers. *J. Chem. Phys.* **144**, 024115 (2016).
60. E. Bertin, A. Baskaran, H. Chaté, M. C. Marchetti, Comparison between Smoluchowski and Boltzmann approaches for self-propelled rods. *Phys. Rev. E* **92**, 042141 (2015).
61. S. A. Mallory, A. K. Omar, J. F. Brady, Dynamic overlap concentration scale of active colloids. *Phys. Rev. E* **104**, 044612 (2021).
62. P. Digregorio *et al*., Full phase diagram of active Brownian disks: From melting to motility-induced phase separation. *Phys. Rev. Lett.* **121**, 098003 (2018).
63. A. K. Omar, K. Klymko, T. GrandPre, P. L. Geissler, Phase diagram of active Brownian spheres: Crystallization and the metastability of motility-induced phase separation. *Phys. Rev. Lett.* **126**, 188002 (2021).
64. J. T. Siebert *et al*., Critical behavior of active Brownian particles. *Phys. Rev. E* **98**, 030601(R) (2018).
65. Z. You, A. Baskaran, M. C. Marchetti, Nonreciprocity as a generic route to traveling states. *Proc. Natl. Acad. Sci. U.S.A.* **117**, 19767–19772 (2020).
66. S. Saha, J. Agudo-Canalejo, R. Golestanian, Scalar active mixtures: The nonreciprocal Cahn-Hilliard model. *Phys. Rev. X.* **10**, 041009 (2020).
67. A. Dinelli *et al.* Non-reciprocity across scales in active mixtures. arXiv [Preprint] (2022). http://arxiv.org/abs/2203.07757 [cond-mat.stat-mech] Accessed 23 December 2022.
68. Y. J. Chiu, A. K. Omar, Phase Coexistence Implications of Violating Newton's Third Law. arXiv [Preprint] (2022). http://arxiv.org/abs/2212.03995 [cond-mat.soft] Accessed 15 February, 2023.
69. J. D. Weeks, D. Chandler, H. C. Andersen, Role of repulsive forces in determining the equilibrium structure of simple liquids. *J. Chem. Phys.* **54**, 5237–5247 (1971).
70. J. A. Anderson, J. Glaser, S. C. Glotzer, HOOMD-blue: A Python package for high-performance molecular dynamics and hard particle Monte Carlo simulations. *Comput. Mater. Sci.* **173**, 109363 (2020).
71. J. Lekner, J. R. Henderson, Theoretical determination of the thickness of a liquid-vapour interface. *Physica A* **94**, 545–558 (1978).